




Thermal conductivity of rare-earth titanate pyrochlores

Makoto Tachibana ^{1,*}, Ahmad Rifqi Muchtar ^{1,2}, and Takao Mori ^{1,3}

¹International Center for Materials Nanoarchitectonics, National Institute for Materials Science, 1-1 Namiki, Tsukuba 305-0044, Japan

²Institute of Technology Bandung, Bandung 40132, Indonesia

³Graduate School of Pure and Applied Sciences, University of Tsukuba, 1-1-1 Tennoudai, Tsukuba 305-8577, Japan



(Received 15 February 2022; revised 14 April 2022; accepted 15 April 2022; published 26 April 2022)

Pyrochlore oxides with the chemical formula $R_2B_2O_7$ (R = rare earth and B = tetravalent metal) exhibit very low thermal conductivities (κ) and are considered as promising materials for thermal barrier coatings. To achieve better understanding of their intrinsic thermal properties, this study reports κ for single crystalline $Gd_2Ti_2O_7$ and $Dy_2Ti_2O_7$, and for a series of polycrystalline $R_2Ti_2O_7$, in the temperature range from 300 to 773 K. For the single crystals, κ values are evaluated in comparison to spinel $MgAl_2O_4$ and garnet $Y_3Al_5O_{12}$ using the Slack equation. It is more difficult to obtain satisfactory analysis for the pyrochlores, and this is attributed to the strong involvement of low-lying optic phonons and very low energies of zone-boundary acoustic phonons. For polycrystalline $R_2Ti_2O_7$, κ values similar to single crystals are obtained. Comparison with published data shows a systematic trend of $\kappa(R_2Sn_2O_7) > \kappa(R_2Ti_2O_7) > \kappa(R_2Zr_2O_7)$ at 300 K, which reflects the increasing ionicity from Sn^{4+} to Ti^{4+} to Zr^{4+} . For the three $R_2B_2O_7$ systems, κ appears to decrease with either decreasing ionic radius or increasing cation mass of R .

DOI: [10.1103/PhysRevMaterials.6.045405](https://doi.org/10.1103/PhysRevMaterials.6.045405)

I. INTRODUCTION

For the past several decades, 7–8 wt.% yttria stabilized zirconia (YSZ) has been widely used for thermal barrier coatings (TBCs), which are deposited onto the metallic components in the gas turbine to increase the operation temperature and energy efficiency [1,2]. Perhaps due to the strong notion of YSZ as a textbook example [3] of a refractory oxide with low thermal conductivity (κ), there were only sporadic attempts to find better TBCs materials up to the late 1990s. Then, the situation changed around 2000, when Vassen *et al.* [4] reported that $La_2Zr_2O_7$ exhibits a combination of excellent properties for TBCs: a lower κ ($< 2 \text{ W m}^{-1} \text{ K}^{-1}$) than YSZ up to 1773 K, high thermal stability under oxidative condition, and strong compatibility with the substrate material. Thus began the renewed efforts to explore new TBCs materials in general [5] and low κ oxides in particular [6]. As was predicted by Clarke and Phillpot in 2005 [7], κ research has once again become an active topic in ceramics science, with strong current emphasis on microscopic understanding aided by recent advances in computational physics [8].

$La_2Zr_2O_7$, which started this excitement, belongs to the family of rare-earth $R_2B_2O_7$ pyrochlores [9], where R is a trivalent rare earth and B is a tetravalent metal such as Zr^{4+} , Ti^{4+} , Sn^{4+} , and Pb^{4+} . With the space group of $Fd\bar{3}m$ and $Z = 8$, the cubic pyrochlore structure can be viewed as interpenetrating networks of BO_6 octahedra and R_2O chains, with the R cation being eightfold coordinated with oxygen. It is generally believed that this structure is constrained in the range $1.46 \leq r_R/r_B \leq 1.80$, where r_R and r_B are the ionic

radii [10] of R and B , respectively: $R_2Zr_2O_7$ ($r_{Zr} = 0.72 \text{ \AA}$) is limited to $R = La\text{--}Gd$ as smaller R stabilizes the fluorite-type structure, while $R_2Ti_2O_7$ ($r_{Ti} = 0.605 \text{ \AA}$) is confined to $R = Sm\text{--}Lu$ and Y because larger R leads to the monoclinic structure [9].

The stability of pyrochlore structure suggests various ways to explore beyond $La_2Zr_2O_7$, and indeed κ has been examined on other members of $R_2Zr_2O_7$ [11,12] and on solid solutions at both the R and Zr sites [13,14]. However, aside from a systematic study on $R_2Sn_2O_7$ [15], there have been relatively few experimental efforts to understand κ on other pyrochlore compounds. This is probably due in part to the early molecular dynamics study of Schelling *et al.* [16], which predicted that $R_2Pb_2O_7$, $R_2Zr_2O_7$, and $R_2Sn_2O_7$ should have the lowest κ among pyrochlores ($R_2Pb_2O_7$ are synthesized under high pressure and decompose above $\sim 600 \text{ K}$ in air [9]). Nevertheless, careful κ studies on other members should lead to better understanding of pyrochlores, as they will provide more complete picture for systematically analyzing the thermal transport properties.

With such an objective in mind, this study reports κ for (1) single crystals of $Gd_2Ti_2O_7$ and $Dy_2Ti_2O_7$, and (2) a series of polycrystalline $R_2Ti_2O_7$, in the temperatures $T = 300\text{--}773 \text{ K}$ where κ is largely determined by intrinsic phonon-phonon interactions [17]. In (1), our emphasis is on providing quantitative analysis of κ , through comparison with single crystals of spinel $MgAl_2O_4$ (cubic, space group $Fd\bar{3}m$) and garnet $Y_3Al_5O_{12}$ (cubic $Ia\bar{3}d$) measured under the same condition. These oxides are chosen because their compositional and structural complexities are similar to those of pyrochlores, and also because pertinent material parameters are available for the analysis. In (2), our objective is to examine the change in κ with R for $R_2Ti_2O_7$, and to compare the values with other

*Corresponding author: tachibana.makoto@nims.go.jp

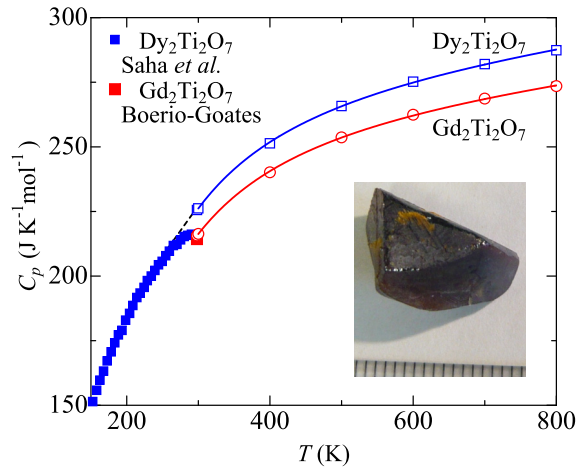


FIG. 1. Heat capacity of $\text{Gd}_2\text{Ti}_2\text{O}_7$ and $\text{Dy}_2\text{Ti}_2\text{O}_7$. Empty symbols are the calculated values from the constituent oxides using the Neumann-Kopp rule. Filled symbols are published data for $\text{Gd}_2\text{Ti}_2\text{O}_7$ [31] and $\text{Dy}_2\text{Ti}_2\text{O}_7$ [32] below 300 K. Inset: Single crystal of $\text{Gd}_2\text{Ti}_2\text{O}_7$. Scale in mm.

systems of $R_2\text{B}_2\text{O}_7$. Together, these results provide significant insights on this important group of compounds.

II. EXPERIMENT

The single crystals of $\text{Gd}_2\text{Ti}_2\text{O}_7$ and $\text{Dy}_2\text{Ti}_2\text{O}_7$ investigated in this study came from the same batch used in Ref. [18], where high-quality crystals of $R_2\text{Ti}_2\text{O}_7$ ($R = \text{Gd}, \text{Tb}, \text{Dy}, \text{Ho}, \text{Er}, \text{Lu}, \text{and Y}$) were grown by the flux method using PbO , PbO_2 , PbF_2 , and MoO_3 as the flux. In the previous study [18], the focus was on low-temperature geometrically frustrated magnetism of R ions, and κ was measured between 2 and 330 K using a Quantum Design physical property measurement system. As this technique suffers from significant radiation loss above 100 K and the measurements were carried out on irregular-shaped crystals, these κ results will not be discussed in the present study. Among the seven $R_2\text{Ti}_2\text{O}_7$ compounds, only the growth runs for $\text{Gd}_2\text{Ti}_2\text{O}_7$ and $\text{Dy}_2\text{Ti}_2\text{O}_7$ yielded crystals that were large enough for the present study; a photograph for $\text{Gd}_2\text{Ti}_2\text{O}_7$, which is extremely large for a flux-grown crystal, is shown in the inset of Fig. 1. (It may be noted here that floating-zone growth yields single crystalline rods of about $\phi 5$ mm, which are not large enough for the present purpose.) The brown color is typical of $R_2\text{Ti}_2\text{O}_7$ crystals grown by various techniques [19,20], and is believed to arise from a minute amount of oxygen deficiency [20]. Colorless single crystals of MgAl_2O_4 and $\text{Y}_3\text{Al}_5\text{O}_{12}$ were also grown by the flux method, using a $\text{PbO-PbF}_2\text{-B}_2\text{O}_3$ flux. These crystals have been characterized and described in previous reports [21,22].

Polycrystalline samples of $R_2\text{Ti}_2\text{O}_7$ ($R = \text{Sm}, \text{Dy}, \text{Ho}, \text{Yb}, \text{and Lu}$) were prepared by solid-state reactions in air. Dried powders of $R_2\text{O}_3$ (99.9%) and TiO_2 (99.999%) were balled milled using ethanol and zirconia balls for 10 h, and calcined at 1373 K for 10 h. The resulting powders were balled milled again, uniaxially pressed into pellets, and fired at 1673 K for 15 h. The fired pellets were again balled milled, pelletized

under an isostatic pressure of 200 MPa, and sintered at 1823 K for 24 h. X-ray powder diffraction confirmed the phase purity of each sample, and the obtained cubic lattice parameters agreed well with the literature values [9,23]. We note that the diffraction patterns for the powdered $\text{Dy}_2\text{Ti}_2\text{O}_7$ crystal and polycrystals were indistinguishable, and the powdered $\text{Gd}_2\text{Ti}_2\text{O}_7$ crystal gave a cubic lattice parameter in good agreement with the literature value.

The κ values were obtained through the relation $\kappa = D\rho C_p$, where D is thermal diffusivity, C_p is heat capacity, and ρ is density. The D between 300 and 773 K was measured in nitrogen atmosphere by the flash method, using Netzsch LFA 467. For the measurements, single crystals were cut into square plates of 6×6 mm² faces and ~ 2 -mm thicknesses, and were coated on both sides with a thin layer of graphite. The plate faces corresponded to cubic {111} for $\text{Gd}_2\text{Ti}_2\text{O}_7$, $\text{Dy}_2\text{Ti}_2\text{O}_7$, and MgAl_2O_4 , and cubic {110} for $\text{Y}_3\text{Al}_5\text{O}_{12}$. The sample preparation for polycrystals was similar, except that the faces of the square plates were 10×10 mm² in size. To account for ballistic radiative transfer (photon conduction) through the samples [24], the model of Mehling *et al.* [25] was used to analyze the temperature-time response in the D measurements. For $R_2\text{Ti}_2\text{O}_7$, C_p was calculated from the weighted sum of the C_p for the constituent oxides $R_2\text{O}_3$ and TiO_2 [26], following the Neumann-Kopp rule. For MgAl_2O_4 and $\text{Y}_3\text{Al}_5\text{O}_{12}$, literature C_p values [27,28] were used. The ρ value was determined using the Archimedes technique. As the ρ of sintered pellets were 87–92% of the theoretical values, the raw κ values (κ_{raw}) were converted to the κ of a fully dense solid through the relation $\kappa_{\text{raw}}/\kappa = 1 - 4\Phi/3$, where Φ is the porosity of the polycrystalline specimen [29]. The overall uncertainty in κ is estimated to be less than $\pm 5\%$.

III. RESULTS AND DISCUSSION

A. Single crystalline data

We first examine the validity of Neumann-Kopp rule (NKR) in obtaining the C_p of pyrochlores. Figure 1 shows both the NKR and literature values of C_p for $\text{Gd}_2\text{Ti}_2\text{O}_7$ and $\text{Dy}_2\text{Ti}_2\text{O}_7$, in units of $\text{JK}^{-1}\text{mol}^{-1}$. The NKR values follow $C_p = a + bT + cT^{-2}$, which are shown with solid lines. At these temperatures, C_p of $\text{Gd}_2\text{Ti}_2\text{O}_7$ arises solely from lattice vibrations, and its value exceeds the Dulong-Petit limit of $C_v = 33R = 274.4 \text{ JK}^{-1}\text{mol}^{-1}$ (C_v is the heat capacity at constant volume and R is the gas constant) above 800 K due to lattice anharmonicity. C_p of $\text{Dy}_2\text{Ti}_2\text{O}_7$ contains an additional contribution from crystal field excitations of Dy^{3+} , in which the first excited doublet appears at 21 meV [30]. For $\text{Gd}_2\text{Ti}_2\text{O}_7$, the NKR value of $215.7 \text{ JK}^{-1}\text{mol}^{-1}$ at 298.15 K agrees well with Boerio-Goates's value of $214.3 \text{ JK}^{-1}\text{mol}^{-1}$, which was reported in Janßen *et al.* [31] as unpublished data. For $\text{Dy}_2\text{Ti}_2\text{O}_7$, Saha *et al.* [32] obtained C_p up to 290 K using a relaxation method. As can be seen from the plot, the data show anomalous saturating behavior above ~ 260 K, which is attributed to the anomaly of Apizeon N grease [33] used in the measurement [32]. However, when their C_p below 260 K is extrapolated to 300 K (dashed line in Fig. 1), it joins smoothly with the NKR value. Therefore, these observations provide

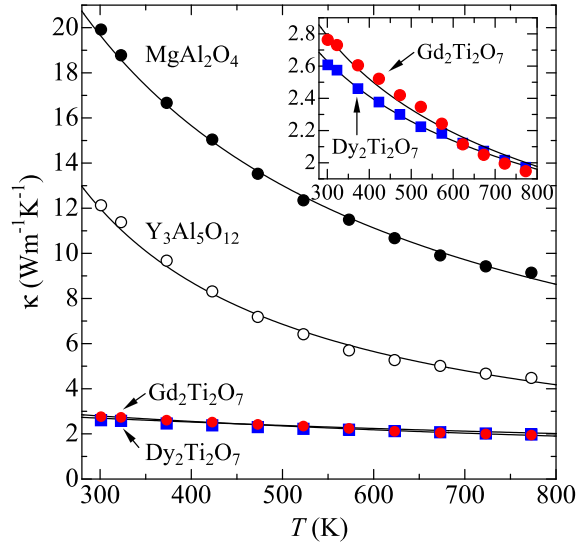


FIG. 2. Thermal conductivity of $\text{Gd}_2\text{Ti}_2\text{O}_7$, $\text{Dy}_2\text{Ti}_2\text{O}_7$, MgAl_2O_4 , and $\text{Y}_3\text{Al}_5\text{O}_{12}$ single crystals. Solid lines are fit to $\kappa = (A + BT)^{-1}$. Inset: The same data for $\text{Gd}_2\text{Ti}_2\text{O}_7$ and $\text{Dy}_2\text{Ti}_2\text{O}_7$ in an expanded κ scale. Solid lines are fit to $\kappa = B'T^{-\alpha}$ with $\alpha = 0.35$ and 0.30 , respectively.

confidence in using NKR for the C_p of pyrochlore $R_2\text{Ti}_2\text{O}_7$ compounds.

The κ for $\text{Gd}_2\text{Ti}_2\text{O}_7$, $\text{Dy}_2\text{Ti}_2\text{O}_7$, MgAl_2O_4 , and $\text{Y}_3\text{Al}_5\text{O}_{12}$ single crystals are shown in Fig. 2. In the inset, the same data for $\text{Gd}_2\text{Ti}_2\text{O}_7$ and $\text{Dy}_2\text{Ti}_2\text{O}_7$ are plotted in an expanded κ scale. At 300 K, our MgAl_2O_4 value of $20 \text{ Wm}^{-1} \text{ K}^{-1}$ is in good agreement with the previous values of $20\text{--}24 \text{ Wm}^{-1} \text{ K}^{-1}$ [34–36]. Similarly, our $\text{Y}_3\text{Al}_5\text{O}_{12}$ value of $12 \text{ Wm}^{-1} \text{ K}^{-1}$ falls within the range $10\text{--}13 \text{ Wm}^{-1} \text{ K}^{-1}$ reported previously [37–40]. Compared to these compounds, much smaller κ are observed in $\text{Gd}_2\text{Ti}_2\text{O}_7$ and $\text{Dy}_2\text{Ti}_2\text{O}_7$. For $\text{Gd}_2\text{Ti}_2\text{O}_7$, our value of $2.8 \text{ Wm}^{-1} \text{ K}^{-1}$ is comparable to $2.9 \text{ Wm}^{-1} \text{ K}^{-1}$ reported on a polycrystalline sample [29]. Also, a single crystalline value of $2.4 \text{ Wm}^{-1} \text{ K}^{-1}$ has been reported for $\text{Tb}_2\text{Ti}_2\text{O}_7$ [19]; however, the data show anomalous upturn beginning above $\sim 500 \text{ K}$, signifying spurious contributions from ballistic radiative transfer [24].

As expected for phonon transport in electrically insulating crystals, each compound in Fig. 2 shows monotonic decrease in κ with increasing temperature. These data can be empirically fitted with $\kappa = (A + BT)^{-1}$, and the results are shown as solid lines in the main panel of Fig. 2 and as values of A and B in Table I. Typically, such a fit is explained by the coefficient B expressing the T^{-1} dependence of three-phonon anharmonic Umklapp scattering, whereas the coefficient A represents the scattering of phonons by impurities and paramagnetic ions [41,42]. For MgAl_2O_4 , the obtained B gives $BT^{-1} = 26 \text{ Wm}^{-1} \text{ K}^{-1}$ at 300 K. As this value is slightly larger than the reported values of $20\text{--}24 \text{ Wm}^{-1} \text{ K}^{-1}$ [34–36], it may as well represent the κ of a “perfect” MgAl_2O_4 crystal. On the other hand, the negative A value for $\text{Y}_3\text{Al}_5\text{O}_{12}$ indicates that such an explanation does not hold for this compound. Instead, it suggests deviation of the phonon-phonon scattering contribution from a strict T^{-1} dependence, at least in the present temperature range. Indeed, the κ data for $\text{Y}_3\text{Al}_5\text{O}_{12}$ can also

TABLE I. Physical parameters of the four compounds. Definitions for the symbols and sources for the values can be found in the main text.

	MgAl_2O_4	$\text{Y}_3\text{Al}_5\text{O}_{12}$	$\text{Gd}_2\text{Ti}_2\text{O}_7$	$\text{Dy}_2\text{Ti}_2\text{O}_7$
A ($10^{-2} \text{ mK W}^{-1}$)	1.18	−1.03	25.7	30.8
B (10^{-4} mW^{-1})	1.30	3.12	3.35	2.61
n	14	80	22	22
\bar{M} (u)	20.33	29.68	47.49	48.43
δ (Å)	2.11	2.21	2.29	2.28
γ	1.4	1.4	1.9	2.0
θ_D (K)	850	750	568	567
θ_a (K)	352	174	203	202
κ_{calc} ($\text{Wm}^{-1} \text{ K}^{-1}$)	25	8.2	7.2	6.4
κ_{exp} ($\text{Wm}^{-1} \text{ K}^{-1}$)	20	12	2.8	2.6
ω_{TA} (meV)	24.0	12.7		6.56, 7.97
ω_{LA} (meV)	40.7	13.6		13.4
θ'_a (K)	309	151		92

be fitted well by $B'T^{-1.05}$, and such a departure from T^{-1} dependence can arise from higher four-phonon scattering, as well as a change in sample volume and C_p with temperature [43].

For $\text{Gd}_2\text{Ti}_2\text{O}_7$ and $\text{Dy}_2\text{Ti}_2\text{O}_7$, the fit to $(A + BT)^{-1}$ yields a very large A , and the BT^{-1} gives 10 and $13 \text{ Wm}^{-1} \text{ K}^{-1}$, respectively, at 300 K. As these BT^{-1} values are more than three times the experimental κ for all $R_2\text{Ti}_2\text{O}_7$ (see Fig. 4), the A values are too large to be ascribed to impurities or paramagnetic scattering from Gd^{3+} and Dy^{3+} ions. Accordingly, we deem the $(A + BT)^{-1}$ fit to be unphysical, and the κ should instead be interpreted to exhibit a weak temperature dependence; as shown in the inset, the data for $\text{Gd}_2\text{Ti}_2\text{O}_7$ and $\text{Dy}_2\text{Ti}_2\text{O}_7$ can be fitted to $B'T^{-\alpha}$ with $\alpha = 0.35$ and 0.30 , respectively.

We attribute the weak temperature dependence of κ to the short phonon mean free path (l) ($< 1 \text{ nm}$ at 300 K for $R_2\text{Ti}_2\text{O}_7$ [44]), which is also reflected in the low κ that are only slightly higher than the calculated minimum thermal conductivity κ_{min} of $\sim 1.0\text{--}1.2 \text{ Wm}^{-1} \text{ K}^{-1}$ [44]. Here, κ_{min} corresponds to the situation where l is only of the length of interatomic spacing, at which κ becomes temperature independent [45]. It should be noted that the low and weakly temperature dependent κ is similarly observed in $\text{La}_2\text{Zr}_2\text{O}_7$. For this compound, Luo *et al.* [46] have shown recently that κ is contributed mostly by normal phonons (those described by the Boltzmann transport equation theory) at low and room temperatures, whereas diffusionlike phonons (those described by the diffusion theory) dominate at high temperatures. The same explanation should hold for $R_2\text{Ti}_2\text{O}_7$. The reader is referred to this paper [46] for a detailed discussion on how a conventional phonon picture breaks down at high temperatures in pyrochlores.

B. Analysis of single crystalline data

As the κ at 300 K is dominated by normal phonons in the pyrochlores [46] and MgAl_2O_4 and $\text{Y}_3\text{Al}_5\text{O}_{12}$, we can attempt to evaluate their values using the Slack equation [47,48]. This model assumes that only acoustic phonons contribute to

the transport of heat, and that phonons interact only among themselves via anharmonic Umklapp processes. Under these assumptions, Slack has shown that

$$\kappa = \frac{A\bar{M}\theta_a^3\delta n^{1/3}}{\gamma^2 T}, \quad (1)$$

where \bar{M} is the average mass of an atom in the crystal (in u), θ_a is the high temperature limit of acoustic-mode Debye temperature, δ is the cubic root of the volume per atom (in Å), n is the number of atoms in the primitive unit cell, γ is the high temperature Grüneisen parameter for the acoustic phonons, and $A = (2.43 \times 10^{-8})/[1 - (0.514/\gamma) + (0.228/\gamma^2)]$. In short, θ_a is related to the group velocity of heat-carrying phonons, while γ quantifies the anharmonicity and degree of phonon-phonon interactions [47,48]. Because none of the compounds strictly follow a simple T^{-1} dependence, the Slack equation is expected to provide a semiquantitative analysis of the data at 300 K.

The values of each parameter for the four compounds are listed in Table I. The values for n , \bar{M} , and δ are calculated from crystallographic data. For γ , we follow previous analysis [47,48] and use the thermodynamic γ value at 300 K, which is defined as $\gamma = V\beta K/C_p$. Here, V is the molar volume, β is the volumetric expansion coefficient, and K is the bulk modulus. Such γ values for MgAl_2O_4 and $\text{Y}_3\text{Al}_5\text{O}_{12}$ have been evaluated previously [49,50]. For $\text{Gd}_2\text{Ti}_2\text{O}_7$ and $\text{Dy}_2\text{Ti}_2\text{O}_7$, we use $\beta = 2.8 \times 10^{-5}$ and 3.0×10^{-5} [51] and $K = 187$ and 194 GPa [52], respectively. These K values were obtained by first-principles density functional theory (DFT) calculations using the generalized gradient approximation [52]. The obtained γ for the pyrochlores compare well with the pressure-dependent Raman scattering values on $\text{Dy}_2\text{Ti}_2\text{O}_7$, which are 2.2, 1.7, 0.9, and 2.2 for the four modes studied [32].

Although θ_a can be determined precisely by integrating the acoustic portion of the phonon density of states [47,48], this method is not feasible for the present compounds due to significant overlap between the acoustic and optic phonon branches [53–55]. Accordingly, we use the standard relation $\theta_a = \theta_D n^{-1/3}$, where θ_D is the traditional Debye temperature [47,48,56]. The values of θ_D for MgAl_2O_4 and $\text{Y}_3\text{Al}_5\text{O}_{12}$ come from elastic constant data [36,38], and similar values have been used in Slack's previous analysis [47]. For $\text{Gd}_2\text{Ti}_2\text{O}_7$ and $\text{Dy}_2\text{Ti}_2\text{O}_7$, we use the θ_D values obtained in the DFT calculations [52], which gave elastic constants in excellent agreement with the measured values for $\text{Gd}_2\text{Ti}_2\text{O}_7$ [57]. These θ_D values are thus converted to θ_a , which are then used to calculate κ (κ_{calc}) at 300 K. In Table I, κ_{calc} are listed along the experimental κ (κ_{exp}). For MgAl_2O_4 and $\text{Y}_3\text{Al}_5\text{O}_{12}$, κ_{calc} shows good agreement with κ_{exp} , confirming Slack's original analysis on these compounds [47]. (He obtained slightly different values of κ_{calc} and κ_{exp} .) If the ideal κ_{exp} for perfect MgAl_2O_4 is indeed $26 \text{ W m}^{-1} \text{ K}^{-1}$, as discussed in Sec. III A, the agreement with κ_{calc} becomes even better. In contrast, κ_{calc} is larger than κ_{exp} by more than a factor of two for $\text{Gd}_2\text{Ti}_2\text{O}_7$ and $\text{Dy}_2\text{Ti}_2\text{O}_7$, suggesting inaccuracy in at least one of the parameters used to obtain κ_{calc} .

To locate the source of discrepancy for $\text{Gd}_2\text{Ti}_2\text{O}_7$ and $\text{Dy}_2\text{Ti}_2\text{O}_7$, we consider the validity of using the relation $\theta_a = \theta_D n^{-1/3}$. This relation arises from the fact that an increase in n expands the size of the unit cell, which in turn reduces

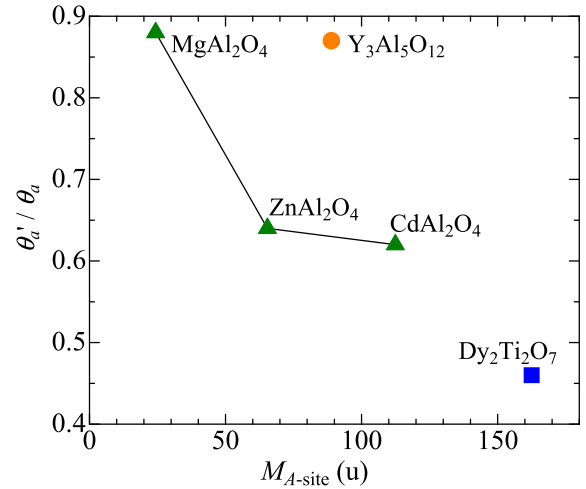


FIG. 3. The ratio θ'_a/θ_a for pyrochlore $\text{Dy}_2\text{Ti}_2\text{O}_7$, spinel MgAl_2O_4 , ZnAl_2O_4 , and CdAl_2O_4 , and garnet $\text{Y}_3\text{Al}_5\text{O}_{12}$ plotted as a function of the A-site cation mass. The first four compounds have a face-centered-cubic lattice, whereas $\text{Y}_3\text{Al}_5\text{O}_{12}$ has a body-centered-cubic lattice.

the Brillouin zone; as the zone boundary moves inward, the acoustic phonon branches are cut off at smaller energies, lowering the value of θ_a [47,48]. However, this relation does not take into account the shape of phonon dispersion, and it can overestimate θ_a if the dispersion flattens considerably near the zone boundary: such an effect is expected to be strong for the pyrochlores, where the mass ratio between the R and oxygen ions is very large. For $\text{Dy}_2\text{Ti}_2\text{O}_7$, we can test it explicitly by taking the average of the published phonon dispersion relations for $\text{Tb}_2\text{Ti}_2\text{O}_7$ and $\text{Ho}_2\text{Ti}_2\text{O}_7$ [53], the neighboring compounds of $\text{Dy}_2\text{Ti}_2\text{O}_7$. From such data, we locate the zone-boundary energies of the longitudinal (ω_{LA}) and two transverse ($\omega_{\text{TA1}}, \omega_{\text{TA2}}$) acoustic phonon branches, which are listed in Table I. These values are then converted to the Debye temperature θ_i of each acoustic branch i ($i = \text{LA, TA1, TA2}$), through $\theta_i = \hbar\omega_i/k_B$ where \hbar is the Planck constant and k_B is the Boltzmann constant [58,59]. Finally, the new acoustic Debye temperature θ'_a is defined [58,59] as the isotropic average $3\theta'^{-3}_a = \theta_{\text{LA}}^{-3} + \theta_{\text{TA1}}^{-3} + \theta_{\text{TA2}}^{-3}$, from which we obtain $\theta'_a = 92$ K for $\text{Dy}_2\text{Ti}_2\text{O}_7$. Now, this θ'_a is too low to be the “correct” acoustic Debye temperature, as it leads to a calculated κ of $0.61 \text{ W m}^{-1} \text{ K}^{-1}$, which is only 23% of κ_{exp} . Nevertheless, the large discrepancy between θ'_a and θ_a (where $\theta'_a/\theta_a = 0.46$) does confirm the inadequacy of using the relation $\theta_a = \theta_D n^{-1/3}$ for the pyrochlores.

Since calculated phonon dispersions are available for MgAl_2O_4 [54] and $\text{Y}_3\text{Al}_5\text{O}_{12}$ [55], as well as for ZnAl_2O_4 [60] and CdAl_2O_4 [61] spinels (for which calculated θ_D are also available [62,63]), it is of interest to examine the ratio θ'_a/θ_a for these compounds as well. The results for the five compounds are plotted as a function of A-site cation mass ($M_{\text{A-site}}$) in Fig. 3, the A-site cation being Dy, Mg, Y, Zn, or Cd in the present compounds. For MgAl_2O_4 and $\text{Y}_3\text{Al}_5\text{O}_{12}$, the values of θ_a , ω_{TA} , and ω_{LA} are listed in Table I. (The two TA modes are degenerate in these compounds. Also, the zone boundary is at the X point of Brillouin zone in pyrochlore

and spinel, whereas it corresponds to the H point in garnet $\text{Y}_3\text{Al}_5\text{O}_{12}$.) From Fig. 3, we find that θ'_a/θ_a is close to unity for MgAl_2O_4 and $\text{Y}_3\text{Al}_5\text{O}_{12}$. These results help to explain why using the value of θ_a led to κ_{calc} in good agreement with κ_{exp} for these compounds. It is also evident from Fig. 3 that the ratio θ'_a/θ_a for the spinel series decreases with increasing $M_{A\text{-site}}$, and roughly extrapolates to the value at $\text{Dy}_2\text{Ti}_2\text{O}_7$. Therefore, this observation identifies the heavy Dy ion as the source of overestimated θ_a and κ_{calc} in $\text{Dy}_2\text{Ti}_2\text{O}_7$. The reason $\text{Y}_3\text{Al}_5\text{O}_{12}$ deviates from the trend can be traced to its body-centered-cubic lattice, which is different from the face-centered-cubic lattice of spinels and pyrochlores.

Although the Slack equation assumes that only acoustic phonons contribute to the transport of heat, it has been applied successfully to a variety of complex compounds. For example, the cubic clathrates (such as $\text{Ba}_8\text{Ga}_{16}\text{Ge}_{30}$) have $\kappa \sim 1 \text{ Wm}^{-1} \text{ K}^{-1}$, $n = 54$, and optic modes that strongly overlap with the acoustic modes [64], yet κ_{calc} shows good agreement with κ_{exp} for a series of 19 compositions [65]. Evidently, the parameter γ is flexible enough to incorporate the effects of interactions between acoustic and optic phonons, which are expected to be strong in systems with significant overlap in the dispersion relations. For $\text{Tb}_2\text{Ti}_2\text{O}_7$ and $\text{Ho}_2\text{Ti}_2\text{O}_7$, the low-lying optic modes have energies as low as 5 meV, which strongly overlap with the acoustic modes [53]. MgAl_2O_4 and $\text{Y}_3\text{Al}_5\text{O}_{12}$ do not show such a severe overlap [54,55], and this difference may be adequate to explain why γ is larger in the pyrochlores. Indeed, first-principles calculations on different pyrochlores [46,66] have produced dispersion relations that closely resemble those of $\text{Tb}_2\text{Ti}_2\text{O}_7$ and $\text{Ho}_2\text{Ti}_2\text{O}_7$, and the low κ and short l were attributed to the interference between the phonons of low-lying optic branches and acoustic branches [46,66]. Intriguingly, a separate first-principles study on $\text{La}_2\text{Sn}_2\text{O}_7$ and $\text{Gd}_2\text{Sn}_2\text{O}_7$ [67] detected optic phonons as significant carriers of heat. There is no doubt that rich physics is involved in the thermal transport of pyrochlores, and it is of interest for further studies to explore the extent to which the Slack equation can accommodate such complex behaviors.

C. Polycrystalline data

We now shift our focus to the κ of polycrystalline $R_2\text{Ti}_2\text{O}_7$, which are presented in Fig. 4. In the figure, the polycrystalline data for $\text{Gd}_2\text{Ti}_2\text{O}_7$ by Liu *et al.* [29], as well as our single crystalline data for $\text{Gd}_2\text{Ti}_2\text{O}_7$ and $\text{Dy}_2\text{Ti}_2\text{O}_7$, are also shown. The first thing to notice is the similarity in κ between the polycrystalline and single crystalline data, in both the magnitude and temperature dependence. This is ascribed to the short length scale of l in the present temperature range, which is $< 1 \text{ nm}$ [44] in the pyrochlores as discussed in Sec. III A; because grain boundaries in polycrystals have diameters $\sim 10^3$ larger than l , they do not contribute significantly to phonon scattering. Among the polycrystalline samples, there are some variations in the temperature dependence above $\sim 500 \text{ K}$, especially between $\text{Ho}_2\text{Ti}_2\text{O}_7$, $\text{Yb}_2\text{Ti}_2\text{O}_7$, and $\text{Lu}_2\text{Ti}_2\text{O}_7$. It is not clear whether such behavior is intrinsic or due to some error in obtaining κ . Possible sources for the latter include inadequacy of the NKR in estimating the C_p at high temperatures, and increasing error in the temperature-time response

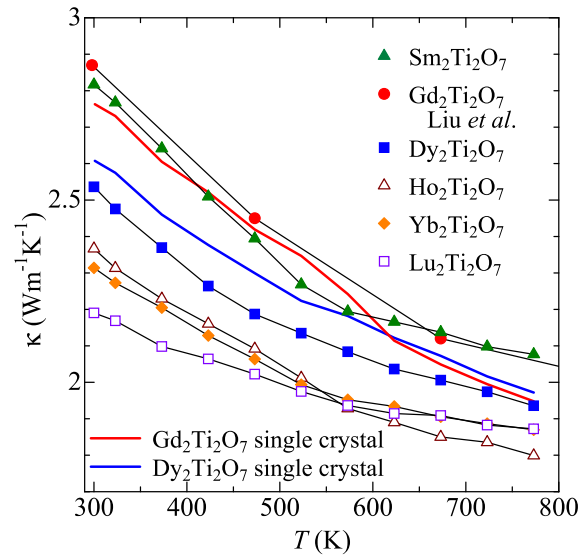


FIG. 4. Thermal conductivity of polycrystalline $R_2\text{Ti}_2\text{O}_7$ ($R = \text{Sm}, \text{Gd}, \text{Dy}, \text{Ho}, \text{Yb}, \text{and Lu}$) and single crystalline $\text{Gd}_2\text{Ti}_2\text{O}_7$ and $\text{Dy}_2\text{Ti}_2\text{O}_7$. The data for polycrystalline $\text{Gd}_2\text{Ti}_2\text{O}_7$ are taken from Ref. [29].

analysis of D at high temperatures. Below, we limit our discussion to the 300 K values, where the κ data are expected to be most reliable.

In Fig. 5, we plot κ at 300 K for polycrystalline $R_2\text{Ti}_2\text{O}_7$, as well as for those of $R_2\text{Sn}_2\text{O}_7$ [15] and $R_2\text{Zr}_2\text{O}_7$ [12] reported previously. Published values for $\text{Gd}_2\text{Ti}_2\text{O}_7$ [29,68] and $\text{Y}_2\text{Ti}_2\text{O}_7$ [68,69] are also shown with empty triangles. The data are plotted as a function of ionic radius of R (r_R), and the cation mass for selected R are also shown at the top. An important feature of Fig. 5 is that, for a given R , the largest

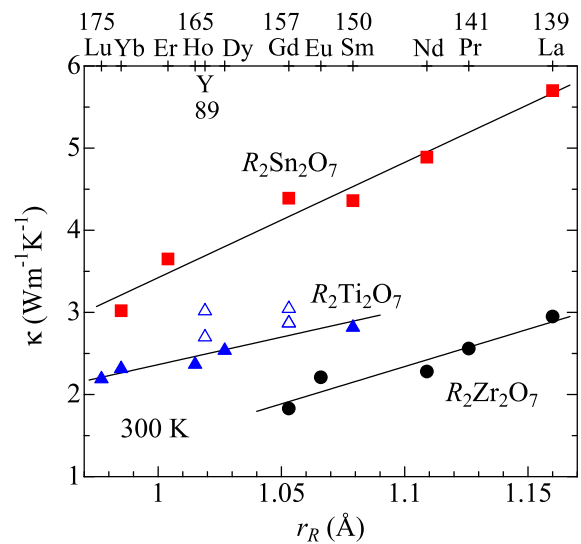


FIG. 5. Thermal conductivity at 300 K for $R_2\text{Sn}_2\text{O}_7$, $R_2\text{Ti}_2\text{O}_7$, and $R_2\text{Zr}_2\text{O}_7$, plotted as a function of ionic radius of R . The data for $R_2\text{Sn}_2\text{O}_7$ [15], $R_2\text{Zr}_2\text{O}_7$ [12], $\text{Gd}_2\text{Ti}_2\text{O}_7$ [29,68], and $\text{Y}_2\text{Ti}_2\text{O}_7$ [68,69] are taken from literature. The lines are drawn to guide the eye. The cation mass (in u) is shown for several R , which is rounded off to a whole number to save space.

κ is found in $R_2\text{Sn}_2\text{O}_7$, followed by $R_2\text{Ti}_2\text{O}_7$ and $R_2\text{Zr}_2\text{O}_7$. The sequence $\kappa_{\text{Sn}} > \kappa_{\text{Ti}} > \kappa_{\text{Zr}}$ is different from that of cation mass ($M_{\text{Sn}} > M_{\text{Zr}} > M_{\text{Ti}}$) or the ionic radius ($r_{\text{Zr}} > r_{\text{Sn}} > r_{\text{Ti}}$), but correlates with the degree of covalent bonding with the oxygen ions, which is $\text{Sn}^{4+} > \text{Ti}^{4+} > \text{Zr}^{4+}$ [70,71]. In Ref. [72], it was shown by first-principles calculations on $\text{La}_2\text{Sn}_2\text{O}_7$ and $\text{La}_2\text{Zr}_2\text{O}_7$ that such a difference in chemical bonds leads to stronger anharmonic potential of the La^{3+} ions in $\text{La}_2\text{Zr}_2\text{O}_7$, resulting in lower κ . Because the Sn^{4+} ion contains filled $4d$ orbitals that are absent in Ti^{4+} and Zr^{4+} , the electronic structure of $R_2\text{Sn}_2\text{O}_7$ is quite different from both $R_2\text{Ti}_2\text{O}_7$ and $R_2\text{Zr}_2\text{O}_7$ [70,71]. Interestingly, this difference is reflected in the κ data, where $R_2\text{Sn}_2\text{O}_7$ show much higher values compared to the other two systems. These results indicate that character of chemical bonds plays a decisive role in κ , and also explain why the earlier molecular dynamics study [16] using simple ionic potentials failed to predict the higher κ in $R_2\text{Sn}_2\text{O}_7$ [15].

Another important feature of Fig. 5 is the similar manner in which κ varies with R for $R_2\text{Sn}_2\text{O}_7$, $R_2\text{Ti}_2\text{O}_7$, and $R_2\text{Zr}_2\text{O}_7$. There are two different ways to look at this result. First, the data may be viewed as a function of r_R , from which κ appears to decrease with decreasing r_R . This observation was already noted for $R_2\text{Sn}_2\text{O}_7$ [15] and $R_2\text{Zr}_2\text{O}_7$ [12]. For $\text{Y}_2\text{Ti}_2\text{O}_7$, which is positioned between $\text{Dy}_2\text{Ti}_2\text{O}_7$ and $\text{Ho}_2\text{Ti}_2\text{O}_7$, the κ values appear slightly higher but roughly in agreement with such a trend. But viewing the κ data in terms of R ionic radius leads to the following inconsistency: In pyrochlores, both the size of cubic unit cell and R -O and B -O bond distances are reduced with decreasing r_R [23,73]. Because the reduction in these structural parameters stiffens the lattice and increases the phonon group velocity, κ should increase with decreasing r_R , in conflict with the above view. Indeed, first-principles calculations on $R_2\text{Zr}_2\text{O}_7$ ($R = \text{La}, \text{Nd}, \text{Sm}, \text{Gd}$) [66] showed that the phonon group velocity decreases as R changes from La to Gd, which should be attributed to the increasing R cation mass (M_R) in this order.

Therefore, there is another way to view the variation in κ with R , which is to recognize that κ decreases with increasing M_R . This view is readily understood from the general behavior of crystals: the increase in M_R reduces the slope of acoustic phonon dispersion and group velocity, which leads to the reduction in κ . Moreover, the increase in M_R has the effect of reducing the energies of low-lying optic modes in pyrochlores, which magnifies γ and the scattering rate of heat-carrying phonons [66,67]. This view (κ decreasing with increasing M_R) therefore provides a consistent explanation for $R_2\text{Sn}_2\text{O}_7$ and $R_2\text{Zr}_2\text{O}_7$, where κ data are missing for

$R = \text{Y}$. ($\text{Y}_2\text{Zr}_2\text{O}_7$ pyrochlore does not exist.) On the other hand, this view requires the κ of $\text{Y}_2\text{Ti}_2\text{O}_7$ (Y : 88.9 u) to be $\kappa \sim 4.5 \text{ W m}^{-1} \text{ K}^{-1}$, based on the extrapolation of data from much heavier R between Lu (175.0 u) and Sm (150.4 u). The actual κ of $\text{Y}_2\text{Ti}_2\text{O}_7$ is only $\leq 3 \text{ W m}^{-1} \text{ K}^{-1}$, and we have no simple explanation for this discrepancy. To settle the problem of whether κ decreases with decreasing r_R or increasing M_R , detailed first-principles κ studies may be necessary; for example, recent calculations on $\text{La}_3\text{Cu}_3\text{X}_4$ ($X = \text{P}, \text{As}, \text{Sb}, \text{Bi}$) [74] revealed counterintuitive evolution of κ with X , which can only be understood through analysis in the scattering phase space [74].

IV. SUMMARY

We have measured the κ of $R_2\text{Ti}_2\text{O}_7$ pyrochlores, for both single crystals and polycrystalline samples. The results for single crystals, which were closely compared to those of spinel MgAl_2O_4 and garnet $\text{Y}_3\text{Al}_5\text{O}_{12}$, underscore the unusually low κ of pyrochlores. Although the Slack equation predicts the measured κ well for MgAl_2O_4 and $\text{Y}_3\text{Al}_5\text{O}_{12}$, the same cannot be said about the pyrochlores. A reason for this failure may be attributed to the strong involvement of low-lying optic phonons, in addition to the very low energies of zone-boundary acoustic phonons. The κ values for the polycrystalline samples were similar to single crystals, demonstrating that the former provide intrinsic thermal transport data in pyrochlores. The present results for $R_2\text{Ti}_2\text{O}_7$, in combination with previous data on $R_2\text{Sn}_2\text{O}_7$ and $R_2\text{Zr}_2\text{O}_7$, revealed the systematic behavior of κ as a function of both the B and R cations. The sequence $\kappa_{\text{Sn}} > \kappa_{\text{Ti}} > \kappa_{\text{Zr}}$ can be explained with the increasing bond ionicity (decreasing covalency) from Sn^{4+} to Ti^{4+} to Zr^{4+} , which has been reported to increase the anharmonic behavior of R vibrations. The variation of κ with R can be viewed as either a function of r_R (ionic radius) or M_R (cation mass), and there is not yet enough evidence to determine which is more appropriate. Additional first-principles calculations should provide important insights on this matter. As the pyrochlores constitute an important group of oxides with low κ , deeper understanding on their systematic behavior should become useful in designing better thermal barrier coating materials.

ACKNOWLEDGMENTS

This study was supported by the funding from JST-Mirai JPMJMI19A1. A. R. M. acknowledges the NIMS-ICGP program for the Indonesia-Japan mobility grant.

- [1] D. R. Clarke, M. Oechsner, and N. P. Padture, *MRS Bull.* **37**, 891 (2012).
- [2] X. Q. Cao, R. Vassen, and D. Stöver, *J. Eur. Ceram. Soc.* **24**, 1 (2004).
- [3] W. D. Kingery, H. K. Bowen, and D. R. Uhlmann, *Introduction to Ceramics*, 2nd ed. (Wiley, New York, 1976).
- [4] R. Vassen, X. Cao, F. Tietz, D. Basu, and D. Stöver, *J. Am. Ceram. Soc.* **83**, 2023 (2000).

- [5] B. Liu, Y. Liu, C. Zhu, H. Xiang, H. Chen, L. Sun, Y. Gao, and Y. Zhou, *J. Mater. Sci. Technol.* **35**, 833 (2019).
- [6] W. Pan, S. R. Phillpot, C. Wan, A. Chernatynskiy, and Z. Qu, *MRS Bull.* **37**, 917 (2012).
- [7] D. R. Clarke and S. P. Phillpot, *Mater. Today* **8**, 22 (2005).
- [8] L. Lindsay, A. Katre, A. Cepellotti, and N. Mingo, *J. Appl. Phys.* **126**, 050902 (2019).

- [9] M. A. Subramanian, G. Aravamudan, and G. V. S. Rao, *Prog. Solid State Chem.* **15**, 55 (1983).
- [10] R. D. Shannon, *Acta Crystallogr. A* **32**, 751 (1976).
- [11] J. Wu, X. Wei, N. P. Padture, P. G. Klemens, M. Gell, E. García, P. Miranzo, and M. I. Osendi, *J. Am. Ceram. Soc.* **85**, 3031 (2002).
- [12] T. Kawano, H. Muta, M. Uno, Y. Ohishi, K. Kurosaki, and S. Yamanaka, *Mater. Res. Soc. Symp. Proc.* **1514**, 139 (2013).
- [13] M. Zhao, W. Pan, C. Wan, Z. Qu, Z. Li, and J. Yang, *J. Eur. Ceram. Soc.* **37**, 1 (2017).
- [14] F. A. Zhao, H. Y. Xiao, X. M. Bai, Z. J. Liu, and X. T. Zu, *J. Alloy. Compd.* **776**, 306 (2019).
- [15] Z. Qu, C. Wan, and W. Pan, *Acta Mater.* **60**, 2939 (2012).
- [16] P. K. Schelling, S. R. Phillpot, and R. W. Grimes, *Philos. Mag. Lett.* **84**, 127 (2004).
- [17] R. Berman, *Thermal Conduction in Solids* (Oxford University Press, Oxford, 1976).
- [18] M. Tachibana, *Solid State Commun.* **174**, 16 (2013).
- [19] D. Klimm, C. Guguschev, D. J. Kok, M. Naumann, L. Ackermann, D. Rytz, M. Peltz, K. Dupré, M. D. Neumann, A. Kwasniewski, D. G. Schlom, and M. Bickermann, *CrystEngComm* **19**, 3908 (2017).
- [20] Q. J. Li, L. M. Xu, C. Fan, F. B. Zhang, Y. Y. Lv, B. Ni, Z. Y. Zhao, and X. F. Sun, *J. Cryst. Growth* **377**, 96 (2013).
- [21] M. Tachibana, A. Iwanade, and K. Miyakawa, *J. Cryst. Growth* **568–569**, 126191 (2021).
- [22] M. Tachibana, *Beginner's Guide to Flux Crystal Growth* (Springer, Tokyo, 2017).
- [23] J. M. Farmer, L. A. Boatner, B. C. Chakoumakos, M. Du, M. J. Lance, C. J. Rawn, and J. C. Bryan, *J. Alloys Compd.* **605**, 63 (2014).
- [24] M. Pertermann and A. M. Hofmeister, *Am. Min.* **91**, 1747 (2006).
- [25] H. Mehling, G. Hautzinger, O. Nilsson, J. Fricke, R. Hofmann, and O. Hahn, *Int. J. Thermophys* **19**, 941 (1998).
- [26] I. Barin, *Thermochemical Data of Pure Substances* (VCH, Weinheim, 1995).
- [27] S. K. Saxena and G. Shen, *J. Geophys. Res.* **97**, 19813 (1992).
- [28] R. J. M. Konings, R. R. van der Laan, A. C. G. van Genderen, and J. C. van Miltenburg, *Thermochim. Acta* **313**, 201 (1998).
- [29] Z. Liu, J. Ouyang, Y. Zhou, and X. Xia, *Mater. Lett.* **62**, 4455 (2008).
- [30] M. Ruminy, E. Pomjakushina, K. Iida, K. Kamazawa, D. T. Adroja, U. Stuhr, and T. Fennell, *Phys. Rev. B* **94**, 024430 (2016).
- [31] A. Janßen, P. Pöml, O. Beneš, T. Geisler, and R. J. M. Konings, *J. Chem. Thermodyn.* **41**, 1049 (2009).
- [32] S. Saha, S. Singh, B. Dkhil, S. Dhar, R. Suryanarayanan, G. Dhalenne, A. Revcolevschi, and A. K. Sood, *Phys. Rev. B* **78**, 214102 (2008).
- [33] W. Schnelle, J. Engelhardt, and E. Gmelin, *Cryogenics* **39**, 271 (1999).
- [34] G. A. Slack, *Phys. Rev.* **126**, 427 (1962).
- [35] G. A. Slack, *Phys. Rev.* **134**, A1268 (1964).
- [36] S. Burghartz and B. Schulz, *J. Nucl. Mater.* **212–215**, 1065 (1994).
- [37] P. H. Klein and W. J. Croft, *J. Appl. Phys.* **38**, 1603 (1967).
- [38] G. A. Slack and D. W. Oliver, *Phys. Rev. B* **4**, 592 (1971).
- [39] R. L. Aggarwal, D. J. Ripin, J. R. Ochoa, and T. Y. Fan, *J. Appl. Phys.* **98**, 103514 (2005).
- [40] Y. Sato and T. Taira, *Opt. Express* **14**, 10528 (2006).
- [41] J. P. Moore and D. L. McElroy, *J. Am. Ceram. Soc.* **54**, 40 (1971).
- [42] A. T. Nelson, D. R. Rittman, J. T. White, J. T. Dunwoody, M. Kato, and K. J. McClellan, *J. Am. Ceram. Soc.* **97**, 3652 (2014).
- [43] J. P. Moore, R. K. Williams, and R. S. Graves, *Phys. Rev. B* **11**, 3107 (1975).
- [44] C. Bryan, C. A. Whitman, M. B. Johnson, J. F. Niven, P. Murray, A. Bourque, H. A. Dąbkowska, B. D. Gaulin, and M. A. White, *Phys. Rev. B* **86**, 054303 (2012).
- [45] D. R. Clarke, *Surf. Coat. Technol.* **163–164**, 67 (2003).
- [46] Y. Luo, X. Yang, T. Feng, J. Wang, and X. Ruan, *Nat. Commun.* **11**, 2554 (2020).
- [47] G. A. Slack, in *Solid State Physics*, edited by H. Ehrenreich, F. Weitz, and D. Turnbull (Academic Press, New York, 1979), Vol. 34, pp. 1–71.
- [48] D. T. Morelli and G. A. Slack, in *High Thermal Conductivity Materials*, edited by S. L. Shindé, and J. S. Goela, (Springer, Berlin, 2006), pp. 37–68.
- [49] V. Askarpour, M. H. Manghnani, S. Fassbender, and A. Yoneda, *Phys. Chem. Min.* **19**, 511 (1993).
- [50] Y. K. Yogurtçu, A. J. Miller, and G. A. Saunders, *J. Phys. C* **13**, 6585 (1980).
- [51] B. S. Hulbert, S. J. McCormack, K. Tseng, and W. M. Kriven, *Acta Crystallogr. B* **77**, 397 (2021).
- [52] P. K. Verma, Ph.D. thesis, Indian Institute of Science, 2019.
- [53] M. Ruminy, M. N. Valdez, B. Wehinger, A. Bosak, D. T. Adroja, U. Stuhr, K. Iida, K. Kamazawa, E. Pomjakushina, D. Prabhakaran, M. K. Haas, L. Bovo, D. Sheptyakov, A. Cervellino, R. J. Cava, M. Kenzelmann, N. A. Spaldin, and T. Fennell, *Phys. Rev. B* **93**, 214308 (2016).
- [54] G. A. de Wijs, C. M. Fang, G. Kresse, and G. de With, *Phys. Rev. B* **65**, 094305 (2002).
- [55] P. Goel, R. Mittal, N. Choudhury, and S. L. Chaplot, *J. Phys.: Condens. Matter* **22**, 065401 (2010).
- [56] O. L. Anderson, *J. Phys. Chem. Solids* **12**, 41 (1959).
- [57] Y. Luan, Ph.D. thesis, University of Tennessee, 2011.
- [58] D. T. Morelli, J. P. Heremans, and G. A. Slack, *Phys. Rev. B* **66**, 195304 (2002).
- [59] D. T. Morelli and J. P. Heremans, *Appl. Phys. Lett.* **81**, 5126 (2002).
- [60] C. M. Fang, C.-K. Loong, G. A. de Wijs, and G. de With, *Phys. Rev. B* **66**, 144301 (2002).
- [61] A. Candan and G. Uğur, *AIP Conf. Proc.* **1618**, 182 (2014).
- [62] N. J. van der Laag, M. D. Snel, P. C. M. M. Magusin, and G. de With, *J. Eur. Ceram. Soc.* **24**, 2417 (2004).
- [63] A. Bouhemadou, F. Zerarga, A. Almuhayya, and S. Bin-Omran, *Mater. Res. Bull.* **46**, 2252 (2011).
- [64] T. Tadano, Y. Gohda, and S. Tsuneyuki, *Phys. Rev. Lett.* **114**, 095501 (2015).
- [65] M. Beekman and A. VanderGraaff, *J. Appl. Phys.* **121**, 205105 (2017).
- [66] G. Lan, B. Ouyang, and J. Song, *Acta Mater.* **91**, 304 (2015).
- [67] Z. Li, J. Yang, Y. Xing, C. Wan, S. Watanabe, and W. Pan, *J. Am. Ceram. Soc.* **104**, 27 (2021).
- [68] N. Sellami, G. Sattonnay, C. Grygiel, I. Monnet, A. Debelle, C. Legros, D. Menut, S. Miro, P. Simon, J. L. Bechade, and L. Thomé, *Nucl. Instrum. Meth. Phys. Res. B* **365**, 371 (2015).

- [69] S. T. Nguyen, T. Nakayama, H. Suematsu, T. Suzuki, M. Takeda, and K. Niihara, *Ceram. Int.* **42**, 11314 (2016).
- [70] W. R. Panero, L. P. Stixrude, and R. C. Ewing, *Phys. Rev. B* **70**, 054110 (2004).
- [71] J. M. Pruneda and E. Artacho, *Phys. Rev. B* **72**, 085107 (2005).
- [72] Z. Li, Y. Xing, S. Watanabe, and W. Pan, *Ceram. Int.* **46**, 9947 (2020).
- [73] B. J. Kennedy, B. A. Hunter, and C. J. Howard, *J. Solid State Chem.* **130**, 58 (1997).
- [74] T. Pandey, C. A. Polanco, L. Lindsay, and D. S. Parker, *Phys. Rev. B* **95**, 224306 (2017).